The interface adhesion of $CaAlSiN_3$ Eu^{2+} phosphor/silicone used in light-emitting diode packaging: A first principles study

Cui, Zhen; Fan, Jiajie; van Ginkel, Hendrik Joost; Fan, Xuejun; Zhang, Guoqi

DOI
10.1016/j.apsusc.2020.145251

Publication date
2020

Document Version
Final published version

Published in
Applied Surface Science

Applied Surface Science 510 (2020) 145251

Contents lists available at ScienceDirect

Applied Surface Science

journal homepage: www.elsevier.com/locate/apsusc

Full Length Article

The interface adhesion of $CaAlSiN_3$: Eu^{2+} phosphor/silicone used in light-emitting diode packaging: A first principles study

Zhen Cui[a,1], Jiajie Fan[a,b,1], Hendrik Joost van Ginkel[a], Xuejun Fan[c], Guoqi Zhang[a,*]

[a] Department of Microelectronics, Delft University of Technology, Delft 2628 CD, Netherlands
[b] College of Mechanical and Electrical Engineering, Hohai University, Changzhou 213022, China
[c] Department of Mechanical Engineering, Lamar University, PO Box 10028, Beaumont, TX 77710, USA

ARTICLE INFO

Keywords:
$CaAlSiN_3$:Eu^{2+}
Silicone/phosphor interface
Hydrolysis reaction
Adhesion and adsorption
Sliding energy barrier
Moisture

ABSTRACT

The $CaAlSiN_3$:Eu^{2+} red phosphor and its silicone/phosphor composite are very promising materials used in the high color rendering white light-emitting diode (LED) packaging. However, the reliabilities of $CaAlSiN_3$:Eu^{2+} and its composite are still being challenged by phosphor hydrolysis at high humidity application condition. A fundamental understanding of the interface adhesion between silicone and $CaAlSiN_3$:Eu^{2+} is significant for the developments and applications of this material. In this work, the mechanical properties of silicone/pristine $CaAlSiN_3$:Eu^{2+} and silicone/hydrolyzed $CaAlSiN_3$:Eu^{2+} composites are experimentally measured and compared firstly, in which both the tensile strength and Young's modulus of composite are increased after the hydrolysis reaction. Then, the first principles Density Functional Theory (DFT) calculations are used to investigate the adhesion behaviors of the silicone molecular on both the pristine and the hydrolyzed $CaAlSiN_3$[0 1 0] at atomic level. The results show that: (1) The silicone molecular is weakly adsorbed on the pristine $CaAlSiN_3$[0 1 0] via Van der Waals (vdW) interactions, while silicone molecular is much stronger absorbed on the hydrolyzed $CaAlSiN_3$[0 1 0] due to the formation of hydrogen bonding at the interface; (2) The transient state calculations indicate that the sliding energy barrier of silicone on the hydrolyzed $CaAlSiN_3$[0 1 0] is higher than that on the pristine one, as the increased adsorption energy and surface roughness. Generally, the findings in this paper can guide the phosphor selection, storage and process in LED packaging, and also assist in improving the reliability design of LED package used in high moisture condition.

1. Introduction

As a new generation light source, phosphor converted white light-emitting diodes (pc-WLEDs), generally constructing by a blue LED chip coated with the phosphor, are being applied in many fields, like indoor and outdoor lighting, healthcare, automotive headlamp and high-resolution displays and so on [1,2]. In a white LED package, phosphor is an integral part, working as a function of light and color conversion, and its stability directly affects the reliability of white LED [3]. Since phosphors are always sensitive to high temperature and high moisture, the thermal quenching and hydrolysis effects become critical concerns on the phosphor's reliability. Furthermore, phosphor is always mixed within silicone as a light-conversion composite. When the LED operates under harsh application environments, the silicone/phosphor interface is always suffering degradation under conditions of high temperatures [4], high blue light illumination, and high humidity [5–11]. Therefore, the study of interface adhesion in phosphor/silicone composite become one of fundamental researches to improve the reliability of LED package.

In recent years, $CaAlSiN_3$:Eu^{2+} has attracted much attention for its application in warm white or high color rendering [12–14]. It was firstly developed by K. Uheda et al. under a high-temperature and high-pressure solid state reaction with EuN, Ca_3N_2, AlN and Si_3N_4 [15]. The spectrum measurements conducted by Pan. He et al. showed that the excitation and emission spectra of $CaAlSiN_3$:Eu^{2+} phosphors could be effectively excited at 467 nm and exhibit a strong red emission at 668 nm, which indicates the $CaAlSiN_3$:Eu^{2+} phosphor as an excellent candidate for getting red emission for white light-emitting diodes [16]. According to the effective first-principles calculation, the host lattice constants [17], mechanical, electrical and optical properties [18] of $CaAlSiN_3$:Eu^{2+} and its derivatives were predicted. Although phosphors generally have high thermal quenching temperature and good thermal

* Corresponding author.
E-mail address: G.Q.Zhang@tudelft.nl (G. Zhang).
[1] Z Cui contributes to the modeling and simulations; J Fan contributes to the experiments and measurements.

https://doi.org/10.1016/j.apsusc.2020.145251
Received 28 August 2019; Received in revised form 17 November 2019; Accepted 1 January 2020
Available online 03 January 2020
0169-4332/

stability, the reliability of $CaAlSiN_3:Eu^{2+}$ red phosphor is still being challenged by the high humidity application condition. Zhu et al. [19] observed the degradation of $CaAlSiN_3:Eu^{2+}$ in high-temperature and -pressure water stream test, which is explained as the oxidation of both the phosphor host and activator under an oxidant-gas penetration. Our research team also experimentally found the hydrolysis phenomenon of $CaAlSiN_3:Eu^{2+}$ red phosphor, that can lower the crystallinity of $CaAlSiN_3$ and increases its thermal quenching effect [20].

In addition, in a white LED packaging structure, phosphors are always mixed with silicone to form the high-performance composite materials [21]. However, when the phosphors composites are used in the harsh environment (e.g., high temperature and high moisture conditions), the serious lumen degradations and color shifts of a pc-WLED package were observed [22,23]. Luo et al. [7] studied the degradation mechanisms of phosphor/silicone composites used in pc-WLEDs under both high temperature and high humidity conditions. The results show that the hydrolysis of phosphors and the oxidation of silicone under a high moisture environment could accelerate the degradation of phosphor/silicone composites. Moreover, the adhesion behavior between silicone and phosphors is also a serious concern that affects the use of such material in LED packaging. Singh et al. [24] reported the lumen degradation of high-power LEDs aged under high-humidity condition and observed that the voids between silicone and phosphors can promote the adsorption of moisture on silicone, which further could result in subsequent light scattering. However, all current characterizations of phosphors and their silicone composites are studied at macro-level and the understandings on the interactions between phosphor and silicone mainly relay on the characterizations of microstructure and chemical element composition, which cannot provide a deep explanation at atomic level. The explicit physical–chemical effect of humidity condition on the adhesion behavior between silicone and phosphor is still an open question. Those insufficient investigation methods on phosphor/silicone interaction will limit the studies and applications of $CaAlSiN_3:Eu^{2+}$ and its composite.

In this paper, the hydrolyzed $CaAlSiN_3:Eu^{2+}$ red phosphors are obtained via a water immersion experiment, then the pristine and hydrolyzed $CaAlSiN_3:Eu^{2+}$ red phosphors are mixed with silicone to form phosphor/silicone composites respectively. Through tensile tests, their mechanical properties are experimentally obtained and compared. After that, the adhesion properties of silicone molecular on pristine and hydrolyzed surfaces of $CaAlSiN_3$[0 1 0] are investigated by using Density Functional Theory (DFT) calculations. Through comparing the adsorption energy, bonding nature, electronic structures and sliding energy barriers of silicone molecular on both pristine and hydrolyzed $CaAlSiN_3$[0 1 0] surfaces, the hydrolysis effect on the interfacial and mechanical properties of $CaAlSiN_3:Eu^{2+}$/silicone composite are discussed.

2. Experiments and methodology

2.1. Sample preparation and mechanical tests

A commercialized $CaAlSiN_3:Eu^{2+}$ red phosphor is used in this study. The test sample preparation procedure for phosphor/silicone composites is shown in Fig. 1[11,25]: Firstly, red phosphor powders were soaked in deionized water under 55 °C for 1800 s and the hydrolysis reaction was occurred at the surface of phosphor powders as present in Fig. 2. Then, the phosphor powders were filtered and dried from solution. Next, the silicones KJC-1200A and KJC-1200B were mixed with a 1:1 mass ratio. The silicone mixture and the fresh and treated red phosphor powders were thoroughly mixed in a vacuum mixer with mass fractions as 5%, 10%, 15% and 20% respectively. Finally, the phosphor/silicone mixtures were poured into a polyfluortetraethylene mold and cured in a 100 °C oven for 3 h. The geometric dimensions of prepared test samples with a thickness of 1 mm were designed according to the ASTM D1708 standard. The tensile test was conducted by an Electromechanical Universal Testing Machine from the MTS system (China) Co. Ltd (Model: CMT4204, accuracy: level 0.5).

2.2. Computational method

In this study, all first principles calculations were performed based on the density functional theory (DFT) as implemented in the DMol^3 package [26]. The electronic interactions were employed by using the generalized gradient approximation (GGA) with the Perdew-Burke-Ernzerhof (PBE) method [27]. Double numerical basis sets with polarization functions (DNP) were utilized. For geometry optimization calculations, a 5 × 4 × 3 Monkhorst-Pack k-point mesh for the Brillouin zone sampling was used. The convergence criteria of optimized structures are 2×10^{-5} Ha for energy, 0.002 Ha/Å for force, and 5×10^{-3} Å for displacement. Since the chemical elements and composition measurement by using the Energy Dispersive Spectroscopy (EDS) (see the Supplementary Information) indicate that the atomic percentage of Eu element is very small and significantly lower than the other four elements, the host $CaAlSiN_3$ is used in the DFT calculation to investigate the adhesion behavior between silicone and phosphor particle [25]. A unit cell of $CaAlSiN_3$ crystal structure was calculated with 24 atoms, placing two Al atoms and two Si atoms in the four tetrahedral sites, as shown in Fig. 3. When all the structures are fully relaxed by employing the conjugate gradient method, the lattice constants of the unit cell are a = 9.8871 Å, b = 5.7134 Å, and c = 5.1146 Å. These computed parameters are in good agreement with the previous studies [17,18].

Normally, $CaAlSiN_3$ surfaces with three orientations [1 0 0], [0 1 0] and [0 0 1] were reported in previous study [28]. Among these three orientations, the calculations of surface energies show that the $CaAlSiN_3$ [0 1 0] surface has the lowest surface energy (see the Supplementary Information). Thus, to simplify the calculations of all surfaces of $CaAlSiN_3$, the most thermodynamically stable one, $CaAlSiN_3$ [0 1 0] surface, is selected in this study. As shown in Fig. 4(a), the $CaAlSiN_3$[0 1 0] surface was modeled with ten atomic layers of $CaAlSiN_3$ and a thick vacuum layer (> 20 Å) was added in the direction perpendicular to the $CaAlSiN_3$ [0 1 0] surface to ensure the minimum interaction between periodic structures. The bottom two atomic layers of $CaAlSiN_3$ are fixed at their bulk positions, which avoids the effects of broken bonds at the bottom on the surface properties, as shown in the Supplementary Information. After fully relaxing the $CaAlSiN_3$[0 1 0] surface, two water molecules were added to the surface structure to obtain the hydrolyzed $CaAlSiN_3$[0 1 0] surface. Generally, the adhesion behaviors of a common silicone molecular on phosphor surface are very complicated, as in the local area, the adhesion modes are varied from case to case. But such local adhesion behaviors can be understood through the studies of a monomer silicone molecular on phosphor surface at different adsorption sites. Thus, we chose the monomer silicone molecular to study the adhesion property between silicone and $CaAlSiN_3$, as shown in Fig. 4(b).

To investigate the adsorption of the silicone molecular on $CaAlSiN_3$[0 1 0] surface, we first calculated the adsorption energy (E_{ad}) by using the following formulation [29],

$$E_{ad} = E_{silicone/CaAlSiN3} - E_{silicone} - E_{CaAlSiN3}$$

where $E_{silicone/CaAlSiN3}$ is the total energy of silicone/pristine or hydrolyzed $CaAlSiN_3$ structure, $E_{silicone}$ is the energy of silicone molecular, and $E_{CaAlSiN3}$ is the energy of the isolated pristine or hydrolyzed $CaAlSiN_3$ [0 1 0] surfaces. To link the adsorption energy to its electronic structure, we also calculated the charge density of differences for selected adsorption models via [30],

$$\Delta\rho = \rho_{silicone/CaAlSiN3} - \rho_{silicone} - \rho_{CaAlSiN3}$$

where $\rho_{silicone/CaAlSiN3}$, $\rho_{silicone}$ and $\rho_{CaAlSiN3}$ are the total charge density of the optimized silicone/$CaAlSiN_3$ structure, the silicone molecular and the pristine or hydrolyzed $CaAlSiN_3$[0 1 0] surfaces, respectively. In addition, to investigate adhesion behavior of silicone molecular

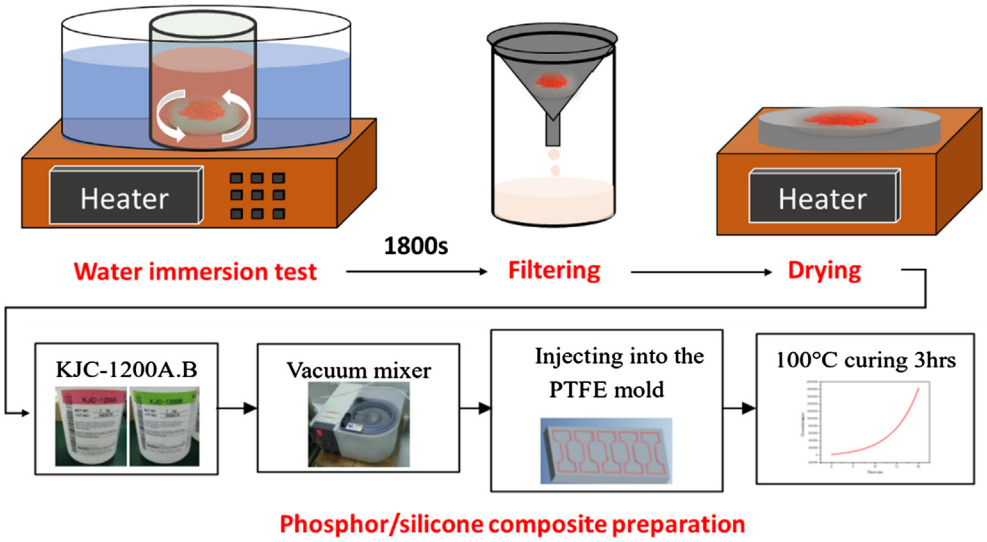

Fig. 1. The test sample preparation procedure for silicone/red phosphor composite.

sliding along $CaAlSiN_3$ surface, the transient state (TS) calculation was conducted to determine the minimum energy pathway and energy barrier by using the method of Linear Synchronous Transit-Quadratic Synchronous Transit (LST-QST) calculation with Conjugate Gradient (CG) minimization [31].

3. Results and discussion

3.1. Simulation results

Before calculating the adhesion of silicone molecular on $CaAlSiN_3$, we first modeled the pristine and hydrolyzed $CaAlSiN_3$[0 1 0] surfaces. Fig. 5(a) displays the fully relaxed pristine $CaAlSiN_3$[0 1 0] surface, the positions of the atoms at the top three layers are slightly changed before and after the optimization. Compared to the Si–N–Al angle in the bulk $CaAlSiN_3$ structure (which is 122.71°), a more open structure with an angle of 152.86°was observed in $CaAlSiN_3$[0 1 0] surface. In this Si—N—Al, the bond length of Si—N decreases from 1.736 Å to 1.693 Å and the bond length of Al—N decreases from 1.872 Å to 1.810 Å. And the position of Ca atom moves closer to the surface after optimization.

On the basis of fully relaxed pristine $CaAlSiN_3$[0 1 0] surface structure, the hydrolyzed surface was obtained as shown in Fig. 3(b). The modeling results show that a chemical reaction occurs at the surface of hydrolyzed $CaAlSiN_3$. The H^+ and OH^- of water molecule are bonded on the surface, forming two N—H bonds with length 1.027 Å, a Si—O bond with distance 1.731 Å and an Al—O bond with length 1.832 Å. Furthermore, the angle of Si—N—Al at the hydrolyzed surface

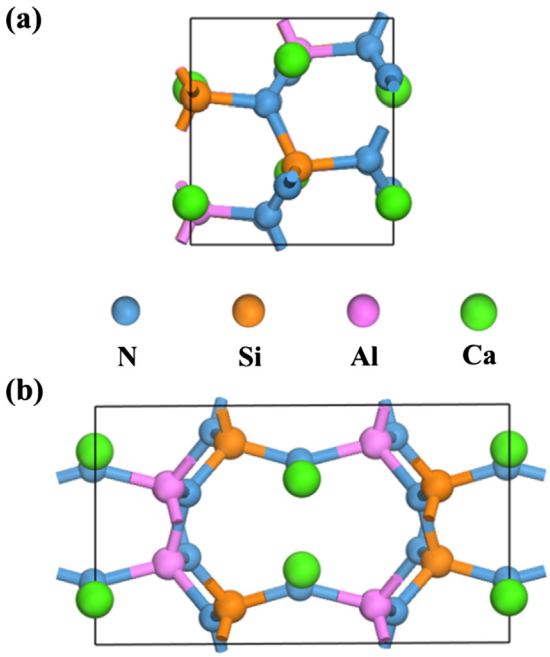

Fig. 3. The crystal structure of $CaAlSiN_3$ along the (a) [0 0 1] and (b) [1 0 0] directions.

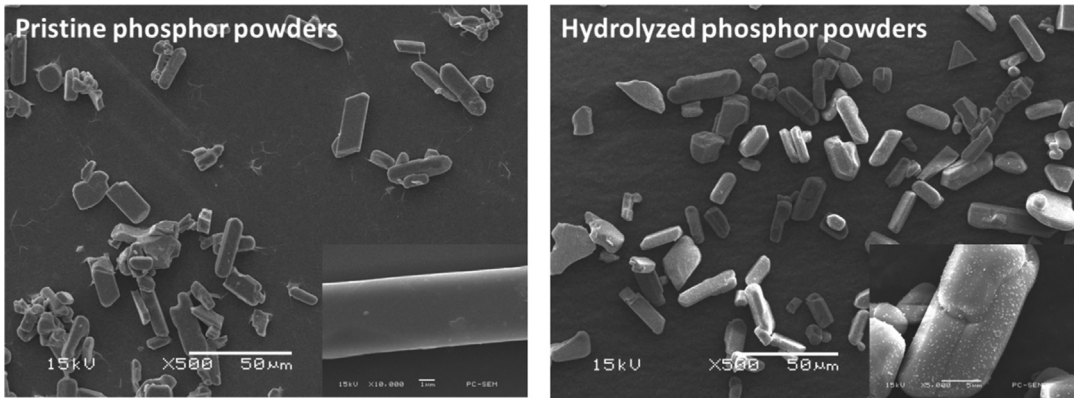

Fig. 2. SEM images of the pristine and hydrolyzed CaAlSiN3:Eu2+ red phosphor powders.

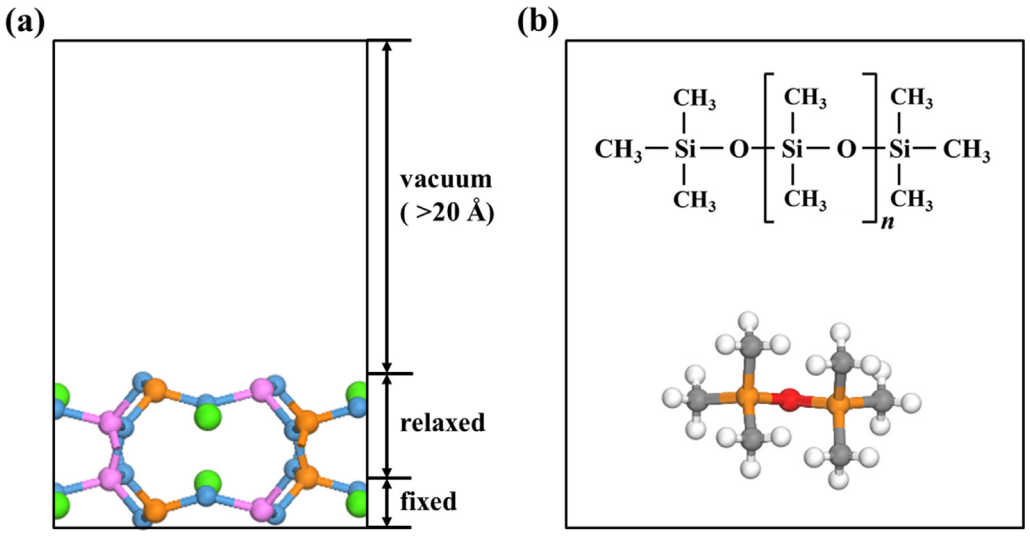

Fig. 4. (a) The schematic diagram of $CaAlSiN_3$[0 1 0] surface structure. (b) The chemical structure of a silicone molecular (top) and the silicone monomer (bottom) used in calculation.

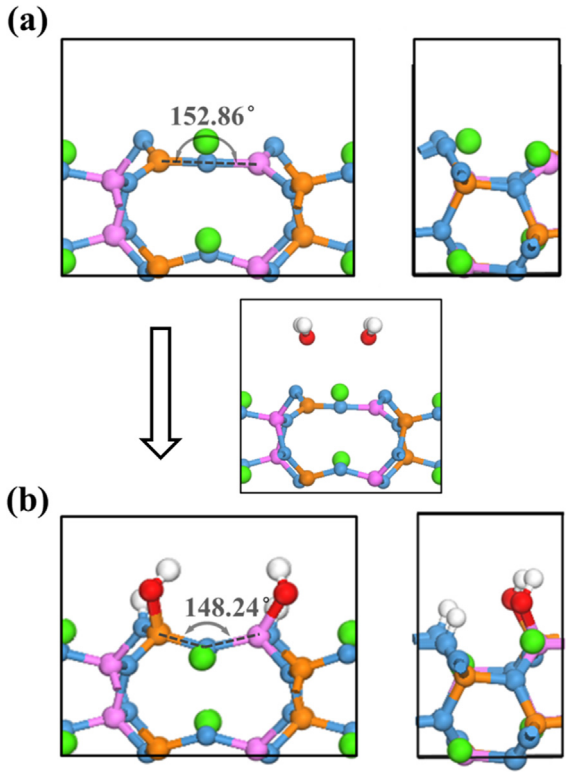

Fig. 5. (a) The optimized pristine $CaAlSiN_3$[0 1 0] surface structure. (b) The optimized hydrolyzed $CaAlSiN_3$[0 1 0] surface structure.

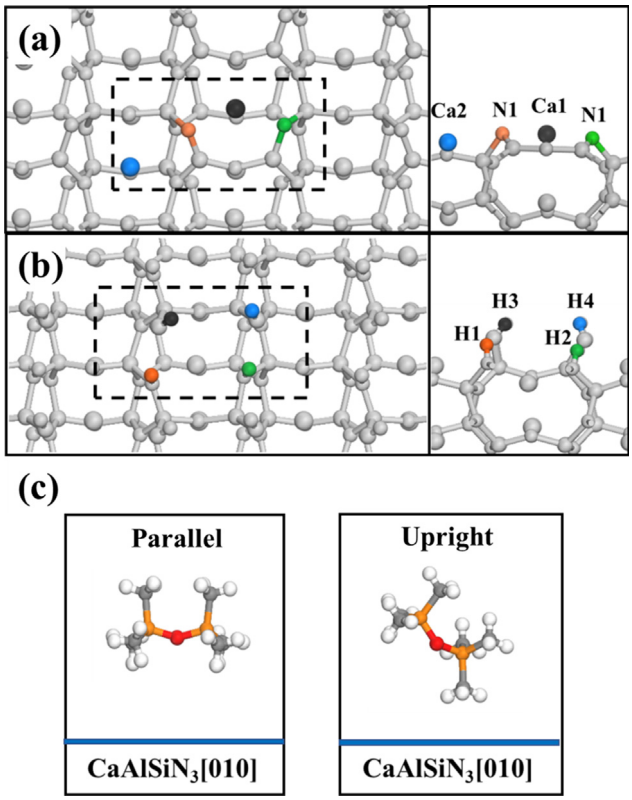

Fig. 6. The top- and side-view of (a) pristine $CaAlSiN_3$[0 1 0] and (b) hydrolyzed $CaAlSiN_3$[0 1 0] surfaces. The unit cell is shown by the black dash lines and the adsorption sites are labeled with various color. (c) The side-view of parallel and upright mode for adsorption.

is 148.24°, smaller than that in pristine surface structure. These different geometry features between hydrolyzed and pristine $CaAlSiN_3$[0 1 0] surfaces suggest that both surfaces may have distinctly different adhesion behaviors to the silicone molecular.

3.1.1. Adsorption of silicone molecular on the pristine and hydrolyzed $CaAlSiN_3$[0 1 0] surfaces

We identify four adsorption sites on the pristine $CaAlSiN_3$[0 1 0] surface as shown in Fig. 6(a), the tops of two N atoms (site-N1 for the orange ball, site-N2 for the green ball) and the tops of two Ca atoms (site-Ca1 for the black ball, site-Ca2 for the blue ball). On the hydrolyzed $CaAlSiN_3$[0 1 0] surface, the tops of H atoms are considered as four adsorptions sites as depicted in Fig. 6(b), site-H1 for the orange ball, site-H2 for the green ball, site-H3 for the black ball and site-H4 for the blue ball.

For the case of silicone adsorption, we modeled the adsorption in two modes: the parallel to the surface and the upright to the surface, as shown in Fig. 6(c). The calculated results for both modes on different sites of pristine and hydrolyzed $CaAlSiN_3$[0 1 0] surfaces are listed in Table 1. It can be seen that the parallel adsorption configurations tend to the higher adsorption energies compared to the upright adsorption

Table 1
Adsorption Energy (E_{ad}), Charge Transfer (ΔQ) from silicone molecular to both surfaces, Shortest Distance (d_{min}) between silicone molecular and surfaces.

	Pristine $CaAlSiN_3$[0 1 0]				Hydrolyzed $CaAlSiN_3$[0 1 0]			
Configuration	Site	E_a (eV)	ΔQ (e)	d_{min} (Å)	Site	E_a (eV)	ΔQ (e)	d_{min} (Å)
Parallel	N1	−1.993	−0.008	2.283	H1	−2.136	−0.035	2.236
	N2	−1.757	0.003	2.391	H2	−2.237	−0.028	2.182
	Ca1	−1.994	−0.003	2.276	H3	−2.195	−0.028	2.248
	Ca2	−1.181	0.027	2.227	H4	−2.159	−0.026	2.053
Upright	N1	−0.850	−0.004	3.221	H1	−1.579	−0.026	2.026
	N2	−0.916	−0.005	3.316	H2	−1.693	−0.015	2.182
	Ca1	−1.144	0.008	2.753	H3	−0.488	-1×10^{-4}	1.931
	Ca2	−1.334	−0.02	2.546	H4	−1.596	−0.004	1.925

mode. The values of charge transfer for the parallel configurations are also higher than the upright mode. We ascribe those preferences to the larger contact area of the parallel mode which promotes the interactions between silicone molecular and the surface. From Table 1, we also can find that no matter what adsorption modes, parallel or upright, the average adsorption energy of silicone molecular on the hydrolyzed surface is higher than that on the pristine surface.

Now, we focus on the most thermodynamically stable adsorptions on pristine $CaAlSiN_3$[0 1 0], namely the parallel model of silicone on site Ca1. As plotted in Fig. 7, the silicone molecular is adsorbed on the surface and oxygen atom moves to the position above Ca atom with distance 2.622 Å. Since the interaction with silicone molecular, the

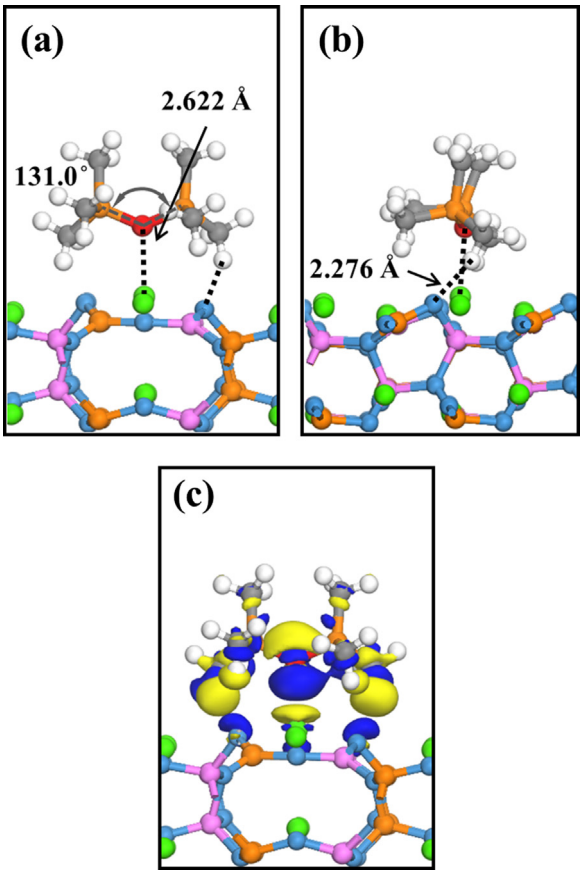

Fig. 7. The thermodynamically most stable adsorption structure of silicone molecular on pristine $CaAlSiN_3$[0 1 0] surface, (a) view along [1 0 0] direction (b) view along [0 0 1] direction. (c) Charge density difference of the silicone/pristine $CaAlSiN_3$[0 1 0] surface, where blue regions represent the charge accumulation and yellow regions mean the charge depletion. The isosurface is taken as 5×10^{-3} e/Å^3. (For interpretation of the references to color in this figure legend, the reader is referred to the web version of this article.)

height of Ca atom is a little bit higher than the other Ca atoms. Four methyl groups of silicone are downward to the surface and the shortest distance is 2.276 Å as the length between H and N atoms. Before and after the adsorption, the angle of Si—O—Si in silicone molecular changes from 136.42° to 131.0°and the length of Si—O bond changes from 1.677 Å to 1.719 Å. The adhesion energy for this configuration is −1.994 eV. The plot of charge density difference shows that the charges are depleted at the Ca atom of $CaAlSiN_3$[0 1 0] and methyl groups of silicone, while the charge accumulation appears at the O atom of silicone and N atoms of $CaAlSiN_3$[0 1 0] as shown in Fig. 7(c). Overall, the total charge transfer of this case is very slight (ΔQ = −0.003 e) and the pristine $CaAlSiN_3$[0 1 0] surface acts as a charge donor and silicone molecular acts as an acceptor. Above calculated adsorption energy and total charge transfer suggest that the silicone molecule is physically adsorbed on the pristine $CaAlSiN_3$ [0 1 0] surface via vdW interactions.

On the hydrolyzed $CaAlSiN_3$[0 1 0] surface, the most stable adsorption site is H2 and the corresponding optimized structure is shown in Fig. 8. The silicone molecular is absorbed on the surface with Si—O—Si parallel to the surface and four methyl groups downward to the surface. The adhesion energy of this configuration is −2.237 eV and the shortest distance between silicone and surface is the length between O and H atoms, 2.182 Å. Before and after the adsorption, the angle of Si—O—Si slightly changes from 136.498° to 136.342°, and the length of Si—O bond increases from 1.677 Å to 1.688 Å. Furthermore, according to the definition of hydrogen bond [32], we find that the silicone molecular is absorbed on the hydrolyzed $CaAlSiN_3$[0 1 0] surface via hydrogen bond O—H···O, as shown in Fig. 8(d). The CDD of this configuration is plotted in Fig. 8(c), an obvious charge transfer between hydroxyl and O atom of silicone is observed, where the charges are accumulated at the side of O atom but depleted at the side of hydroxyl of surface. Generally, the total charge transfer from silicone molecular to surface is −0.028 e and hydrolyzed $CaAlSiN_3$[0 1 0] surface acts as a charge donor and silicone molecular acts as an acceptor. Compare to the vdW interactions between silicone and pristine $CaAlSiN_3$, the hydrogen bonding contributes a stronger intermolecular interaction. Such different bonding nature of silicone on pristine and hydrolyzed $CaAlSiN_3$[0 1 0] surfaces explains the trend, shown in Table 1, that the silicone adsorbs much stronger on hydrolyzed surface.

3.1.2. Sliding of silicone molecular on the pristine and hydrolyzed $CaAlSiN_3$[0 1 0] surfaces

On the basis of thermodynamically most stable adsorptions of silicone on $CaAlSiN_3$[0 1 0] surface, we study the sliding behaviors of silicone on pristine and hydrolyzed surfaces, respectively. On pristine $CaAlSiN_3$[0 1 0] surface, the minimum-energy pathways to slide along [1 0 0] and [0 0 1] directions are plotted in Fig. 9. Along [1 0 0] direction, in one period (from site Ca1 to next site Ca1), the silicone molecular migrates from initial state to intermediate state, passing by the first transit state. Then, the silicone molecular passes the second transit state and finally reaches the final state. The distance of this

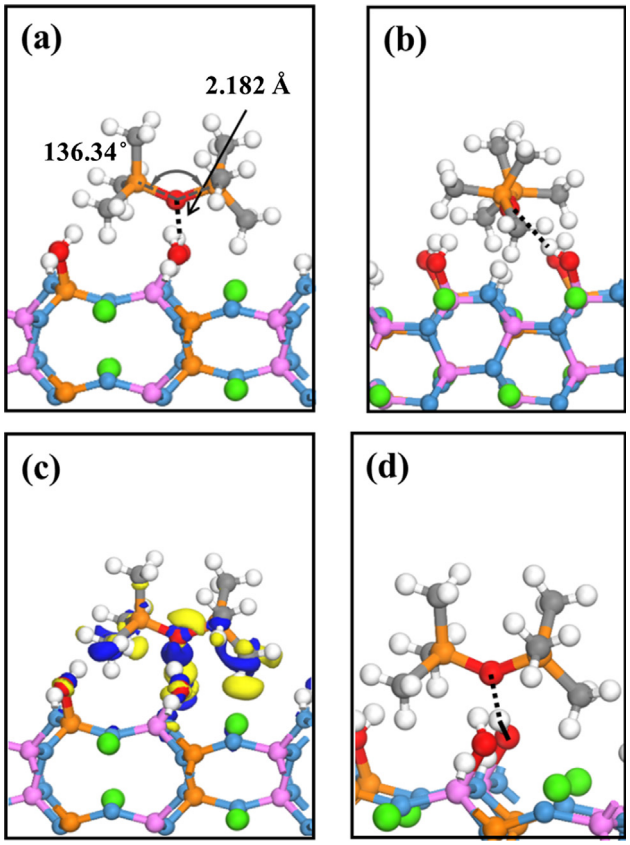

Fig. 8. The thermodynamically most stable adsorption structure of silicone molecular on hydrolyzed $CaAlSiN_3$[0 1 0] surface, (a) view along [1 0 0] direction (b) view along [0 0 1] direction. (c) Charge density difference of the silicone/hydrolyzed $CaAlSiN_3$[0 1 0] surface, the isosurface is taken as 5×10^{-3} e/Å^3. (d) Detail of hydrogen bond, O—H···O.

sliding process is L_1 = 9.88 Å. If we set the energy of the initial state as 0 eV, the energies at first and second transit states are 1.16 eV and 1.07 eV, respectively. On pristine $CaAlSiN_3$[0 1 0], silicone molecular at least requires 1.16 eV to overcome the energy barrier to slide along [1 0 0] direction. In [0 0 1] direction, the silicone molecule passes a transit state and reaches the final state with sliding distance L_2 = 5.71 Å, as shown in Fig. 9(b). The energy barrier along this direction is 1.22 eV.

On the hydrolyzed $CaAlSiN_3$ surface, when silicone slides along [1 0 0] direction, there are two transit states and one intermediate state in one period, as shown in Fig. 10(a). The energies of both transit states are 1.39 eV and 1.40 eV, respectively, so the sliding energy barrier along this direction is 1.40 eV. For the sliding along [0 0 1] direction, the silicone molecular passes a transit state and reaches the final state with energy barrier 1.31 eV, as shown in Fig. 10(b). The embedded pictures in Fig. 10 show that the minimum energy pathways for both directions are passing over the hydroxyls, not through the middle regions between hydroxyls. Compare to the sliding behaviors on pristine $CaAlSiN_3$[0 1 0] surface, the energy barriers along [1 0 0] and [0 0 1] directions at hydrolyzed $CaAlSiN_3$[0 1 0] surface are about 20% and 8% higher than that on pristine $CaAlSiN_3$[0 1 0] surface, respectively. There are two reasons for such differences. Firstly, the hydroxyls bonded on the $CaAlSiN_3$ surface increase the surface roughness, which plays a role as resistance, increasing the friction between the silicone molecular and $CaAlSiN_3$. Secondly, the adhesion energy of silicone on the hydrolyzed $CaAlSiN_3$ surface is higher than that on the pristine surface, so the higher energy is needed to break the adhesion between silicone and hydrolyzed surface. As results, both reasons cause higher energy barriers for the sliding of silicone on hydrolyzed $CaAlSiN_3$[0 1 0].

3.2. Experimental results and explanation

It is well known that the mechanical properties of a composite are dependent on both filler's and matrix's properties and the ability to transfer stresses across the filler/matrix interface [33]. In particular, the ability to transfer stress across the interface is often discussed in terms of 'adhesion', which, in fact, is related to a complex combination of factors, such as the interfacial shear strength [34]. In the tensile test described in part 2.1, the mechanical properties of silicone/hydrolyzed $CaAlSiN_3$:Eu^{2+} composite were obtained and compared to the silicone/pristine $CaAlSiN_3$:Eu^{2+} composite. As plotted in Fig. 11, after hydrolysis reaction, the tensile strength and Young's modulus of silicone $CaAlSiN_3$:Eu^{2+} composite were increased. The SEM images in Fig. 2 show that the hydrolysis reaction mainly occurred at the surface of $CaAlSiN_3$:Eu^{2+} and the microstructure of $CaAlSiN_3$:Eu^{2+} has not dramatically crashed after hydrolysis reaction. Thus, in this experiment, the main difference between hydrolyzed and pristine $CaAlSiN_3$:Eu^{2+}/

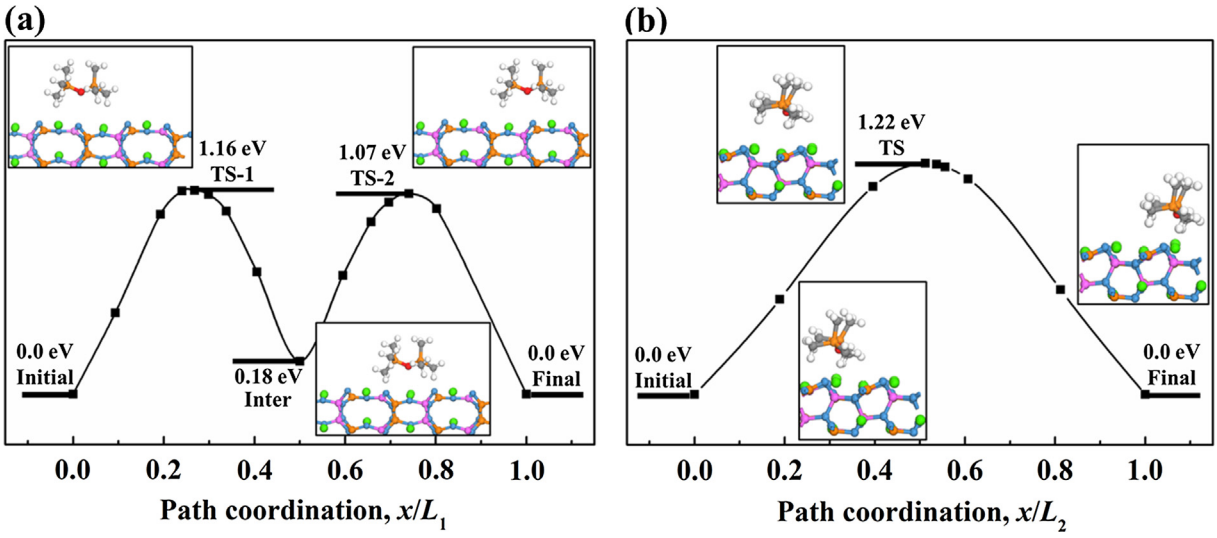

Fig. 9. (a) On pristine CaAlSiN3[0 1 0] surface, the minimum-energy pathway along [1 0 0] direction, L_1 is the sliding distance in one period. (b) minimum-energy pathway along [0 0 1] direction, and L_2 is the sliding distance in one period. The geometry structures at transient states and intermediate state are shown in embedded pictures.

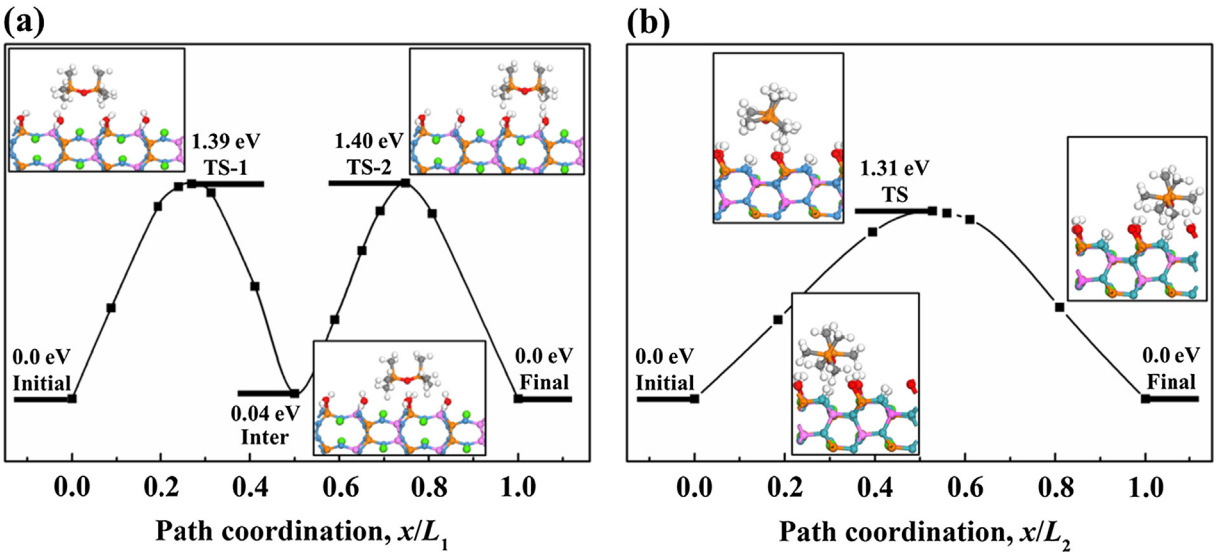

Fig. 10. (a) On pristine $CaAlSiN_3$[0 1 0] surface, the minimum-energy pathway along [1 0 0] direction. (b) On pristine $CaAlSiN_3$[0 1 0] surface, the minimum-energy pathway along [0 0 1] direction. The configurations at transient states and intermediate state are shown in embedded pictures.

silicone composites came from their interfaces. Since SEM characterization shows the rougher surfaces of CaAlSiN3 $CaAlSiN_3:Eu^{2+}$ particles after hydrolysis reaction, so we suspect that the increased friction between silicone and $CaAlSiN_3$ is the major contribution to the enhanced mechanical properties of silicone/$CaAlSiN_3:Eu^{2+}$ composite.

Furthermore, the DFT results in part 3.1 provide a new insight to understand the interface of silicone/$CaAlSiN_3:Eu^{2+}$ at atom level. First, the calculated results showed that the hydrolysis reaction of $CaAlSiN_3$[0 1 0] indeed is able to increase surface roughness, which further leads to the higher sliding energy barrier when silicone slides on $CaAlSiN_3$[0 1 0]. It is implied that the friction on hydrolyzed surface is higher than that on pristine $CaAlSiN_3$[0 1 0] surface. The DFT studies also revealed a possible bonding nature between silicone and hydrolyzed $CaAlSiN_3$[0 1 0]: the hydrogen bond O—H···O. Since the strength of hydrogen bond is obviously higher than the vdW interaction, as a result, the higher adhesion energy is obtained for silicone on hydrolyzed $CaAlSiN_3$[0 1 0]. These simulation results imply that the hydrolysis reaction of $CaAlSiN_3$[0 1 0] can lead to a stronger interface between silicone and $CaAlSiN_3$, which may improve the ability to transfer stress across the interface. Generally, the experimental and simulation results suggest that the hydrolysis reaction of $CaAlSiN_3:Eu^{2+}$ can increase the adhesion strength between silicone and $CaAlSiN_3$ and enhance its composite mechanical properties.

4. Conclusions

In this paper, by using both experimental and theoretical methods, the effects of hydrolysis reaction of $CaAlSiN_3:Eu^{2+}$ on the mechanical and interfacial properties of silicone/ $CaAlSiN_3:Eu^{2+}$ composite are investigated. In experiments, the hydrolysis reaction of $CaAlSiN_3:Eu^{2+}$ increases its surface roughness, and the tensile tests further show that both tensile strength and Young's modulus of silicone/hydrolyzed $CaAlSiN_3:Eu^{2+}$ composite are enhanced after hydrolysis reaction. In DFT studies, we find that the adhesion of silicone molecular on the pristine $CaAlSiN_3$[0 1 0] is the weak physisorption via vdW interaction while the adsorption on the hydrolyzed $CaAlSiN_3$[0 1 0] surface is a more complex bonding nature: hydrogen-bonding of O—H···H. This is well corroborated with the surface electric structures where we clearly observe the corresponding redistribution of charge density on the silicone-$CaAlSiN_3$ interface system. In addition, using the transient state calculations, we reveal that the sliding energy barrier of silicone on hydrolyzed $CaAlSiN_3$[0 1 0] is higher than that on pristine

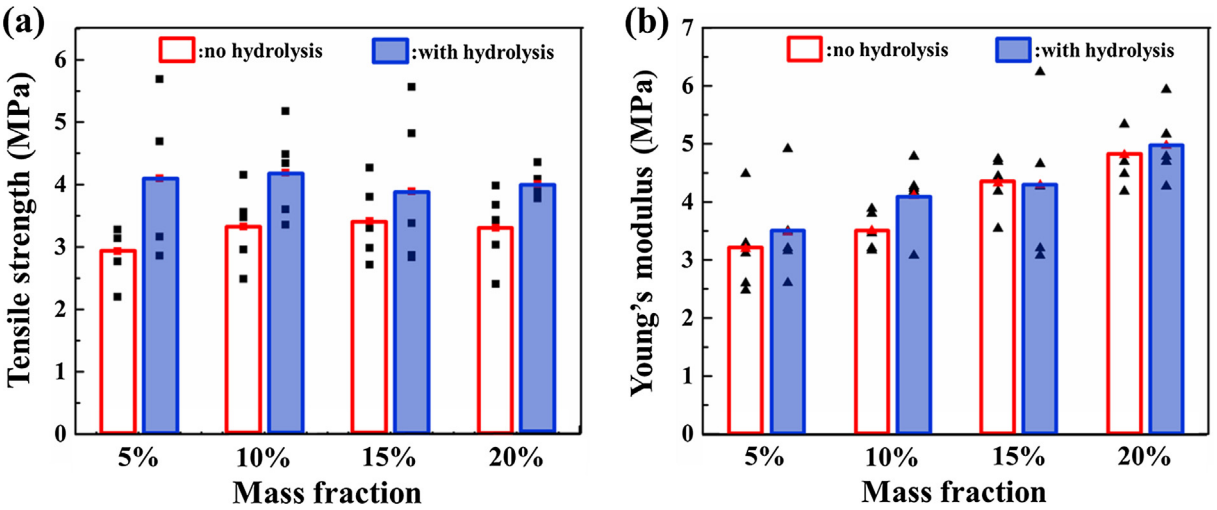

Fig. 11. (a) The tension strength of silicone/phosphor composite with different mass fractions of $CaAlSiN_3$. (b) The Young's modulus of silicone/phosphor composite with different mass fractions of $CaAlSiN_3$.

$CaAlSiN_3$[0 1 0], as the stronger adsorption energy and increased surface roughness. Generally, our experimental and simulation results consistently conclude that the hydrolysis reaction of $CaAlSiN_3$:Eu^{2+} will increase the adhesion of $CaAlSiN_3$: Eu^{2+} phosphor/silicone interface.

Author contribution

Zhen Cui contributes to the modeling and simulations. Jiajie Fan contributes to the experiments and measurements, and provides project administration and funding acquisition. Hendrik Joost van Ginkel contributes the result analysis. Xuejun Fan and Guoqi Zhang support supervision.

Acknowledgements

The work described in this paper was supported by the National Natural Science Foundation of China (Grant No. 51805147).

Appendix A. Supplementary material

Supplementary data to this article can be found online at https://doi.org/10.1016/j.apsusc.2020.145251.

References

[1] W. Van Driel, Solid state lighting reliability: from components to system, in: Proceedings of the China SSL conference, October 2011, Shenzhen, China, 2011.
[2] S. Liu, X. Luo, LED Packaging for Lighting Applications: Design, Manufacturing, and Testing, John Wiley & Sons, 2011.
[3] C.C. Lin, R.-S. Liu, Advances in phosphors for light-emitting diodes, J. Phys. Chem. Lett. 2 (11) (2011) 1268–1277.
[4] Y. Pan, et al., Investigation of mechanical properties of silicone/phosphor composite used in light emitting diodes package, Polymers 10 (2) (2018) 195.
[5] J. Fan, et al., Phosphor–silicone interaction effects in high power white light emitting diode packages, J. Mater. Sci.: Mater. Electron. 28 (23) (2017) 17557–17569.
[6] J. Huang, et al., Rapid degradation of mid-power white-light LEDs in saturated moisture conditions, IEEE Trans. Device Mater. Reliab. 15 (4) (2015) 478–485.
[7] X. Luo, et al., Degradation mechanism analysis for phosphor/silicone composites aged under high temperature and high humidity condition, 2017 18th International Conference on Electronic Packaging Technology (ICEPT), IEEE, 2017.
[8] I. Khalilullah, et al., In-situ characterization of moisture absorption and hygroscopic swelling of silicone/phosphor composite film and epoxy mold compound in LED packaging, 2017 18th International Conference on Thermal, Mechanical and Multi-Physics Simulation and Experiments in Microelectronics and Microsystems (EuroSimE), IEEE, 2017.
[9] M. Choi, et al., Direct correlation between reliability and pH changes of phosphors for white light-emitting diodes, Microelectron. Reliab. 54 (12) (2014) 2849–2852.
[10] P. Singh, C.M. Tan, Degradation physics of high power LEDs in outdoor environment and the role of phosphor in the degradation process, Sci. Rep. 6 (2016) 24052.
[11] J. Fan, et al., High moisture accelerated mechanical behavior degradation of phosphor/silicone composites used in white light-emitting diodes, Polymers 11 (8) (2019) 1277.
[12] S.-X. Li, et al., Synthesis, composition optimization, and tunable red emission of CaAlSiN 3: Eu 2+ phosphors for white light-emitting diodes, J. Mater. Res. 30 (19) (2015) 2919–2927.
[13] C. Cai, et al., Synthesis of red-emitting CaAlSiN3: Eu2+ phosphors through a cost-effective synthetic route, ECS J. Solid State Sci. Technol. 3 (10) (2014) R169–R172.
[14] S.-L. Chung, S.-C. Huang, Combustion synthesis and photoluminescence properties of red-emitting CaAlSiN3: Eu2+ phosphor for white-LEDs, Materials 7 (12) (2014) 7828–7842.
[15] K. Uheda, et al., Luminescence properties of a red phosphor, CaAlSiN3: Eu2+, for white light-emitting diodes, Electrochem. Solid-State Lett. 9 (4) (2006) H22–H25.
[16] P. He, N. Zhang, S. Man, Preparation and properties of Eu doped CaAlSiN3 red phosphor, AIP Conference Proceedings, AIP Publishing, 2017.
[17] S. Jang, et al., First-principles calculation of metal-doped CaAlSiN 3: material design for new phosphors, RSC Adv. 5 (49) (2015) 39319–39323.
[18] Z. Wang, et al., A first-principles study of the electronic structure and mechanical and optical properties of CaAlSiN 3, Phys. Chem. Chem. Phys. 17 (22) (2015) 15065–15070.
[19] J. Zhu, et al., Moisture-induced degradation and its mechanism of (Sr, Ca) AlSiN 3: Eu 2+, a red-color-converter for solid state lighting, J. Mater. Chem. C 3 (13) (2015) 3181–3188.
[20] J.J. Fan, W.Z. Luo, X Degradation mechanism analysis for LED phosphors under hygrothermal environment, Rare Metal Mater. Eng. (2018).
[21] C. Zhaohui, et al., Reliability test and failure analysis of high power LED packages, J. Semicond. 32 (1) (2011) 014007.
[22] B. Sun, et al., A review of prognostic techniques for high-power white LEDs, IEEE Trans. Power Electron. 32 (8) (2016) 6338–6362.
[23] J. Fan, et al., Color shift failure prediction for phosphor-converted white LEDs by modeling features of spectral power distribution with a nonlinear filter approach, Materials 10 (7) (2017) 819.
[24] P. Singh, C.M. Tan, L.-B. Chang, Early degradation of high power packaged LEDs under humid conditions and its recovery—Myth of reliability rejuvenation, Microelectron. Reliab. 61 (2016) 145–153.
[25] Jiajie Fan, Ling Zhou, Zhen Cui, Shanghuan Chen, Xuejun Fan, Guoqi Zhang, Hydrolysis kinetic study of CaAlSiN3:Eu2+ red phosphor with both water immersion test and first-principles calculation, J. Lumin. 219 (2020) 116874, https://doi.org/10.1016/j.jlumin.2019.116874.
[26] B. Delley, An all-electron numerical method for solving the local density functional for polyatomic molecules, J. Chem. Phys. 92 (1) (1990) 508–517.
[27] J.P. Perdew, K. Burke, M. Ernzerhof, Generalized gradient approximation made simple, Phys. Rev. Lett. 77 (18) (1996) 3865.
[28] S. Li, et al., New insights into the microstructure of translucent CaAlSiN 3: Eu 2+ phosphor ceramics for solid-state laser lighting, J. Mater. Chem. C 5 (5) (2017) 1042–1051.
[29] H. Yang, et al., Promoting sensitivity and selectivity of HCHO sensor based on strained InP3 monolayer: a DFT study, Appl. Surf. Sci. 459 (2018) 554–561.
[30] L. Liu, et al., High Selective Gas Detection for small molecules based on Germanium selenide monolayer, Appl. Surf. Sci. 433 (2018) 575–581.
[31] T.A. Halgren, W.N. Lipscomb, The synchronous-transit method for determining reaction pathways and locating molecular transition states, Chem. Phys. Lett. 49 (2) (1977) 225–232.
[32] A. Luzar, D. Chandler, Hydrogen-bond kinetics in liquid water, Nature 379 (6560) (1996) 55.
[33] B.A. Budiman, et al., Modeling of stress transfer behavior in fiber-matrix composite under axial and transverse loadings, Compos. Interfaces 24 (7) (2017) 677–690.
[34] S. Ben, et al., The interface strength and debonding for composite structures: Review and recent developments, Compos. Struct. 129 (2015) 8–26.